Competition of spiral-defect chaos and rolls in Rayleigh-Bénard convection under shear flow

Y. Shiwa*
Statistical Mechanics Laboratory, Kyoto Institute of Technology, Matsugasaki, Sakyo-ku, Kyoto 606-8585, Japan
(Received 1 May 2002; published 10 February 2003)

Computer simulations of domain coarsening of Rayleigh-Bénard convective patterns under horizontal shear flow are carried out. The model calculations reported here explicitly include the hydrodynamic interaction of the order parameter field and provide a description of the spiral-defect chaos which competes with the roll pattern. We observe shear banding at moderate strain rates.

DOI: 10.1103/PhysRevE.67.026306 PACS number(s): 47.54.+r, 47.27.Te, 64.60.Cn, 47.20.Ky

I. INTRODUCTION

Rayleigh-Bénard (RB) convection is a paradigmatic example of spatially extended nonlinear phenomena [1]. When a horizontal fluid layer is heated from below and cooled from above, it undergoes a transition from a spatially and temporally uniform conducting state to a convecting state of lower symmetry. The structure that emerges above the convective threshold in large-aspect-ratio systems is convective rolls (stripes) of arbitrary orientation. When the rolls are distorted into curved textures, curvatures of the patterns induce a horizontal flow. The flow in turn advects the rolls, leading to a nonlocal and long-range hydrodynamic coupling between local structures [2].

As this ''mean flow'' must be divergence-free by effective incompressibility of the fluid, it has only a transverse component. Accordingly, the flow is exclusively described by a (vertical) vorticity field. The chiral nature of the mean flow is then responsible for the formation of passive spirals which were discovered [3] in a small-Prandtl-number fluid at moderate distance from the onset of convection. The pattern is marked by the persistent creation and destruction of rotating spirals of various sizes, and is hence termed spiral-defect chaos (SDC). The discovery was made in a parameter regime where, on the basis of the theory for an infinitely extended system [4], parallel straight rolls (ideal straight rolls, or ISR) are stable. In fact, it has been demonstrated experimentally [5,6] that ISR form only if a perfect parallel-roll pattern is prepared by some special procedures when SDC is the generic attractor from random initial conditions.

Interactions between the flow field and a certain internal structure can also be brought about by shearing of various complex fluids [7]. Examples include liquid crystals, block copolymers, and surfactant solutions. It is well known that the shear has a strong organizing effect upon these systems, and that structures such as lamellae or cylinders are easily aligned by relatively weak shear.

A natural question that arises here is whether SDC can coexist with ISR when both shear and mean flow are present. The aim of this paper is to study this interesting issue. In order to gain insight into the effects of shear on RB convection, we discuss the simplest case of a plane Couette flow, i.e., a flow with the velocity and its gradient in the horizontal plane. [Thermal convection with vertical shear (i.e., shear between parallel plates) has been actively studied in connection with geophysical phenomena such as cloud street formation (see Ref. [8] for a review). However, as far as we know, no work has been done concerning SDC in connection with horizontal shear.] In this case, the rolls will be bent by the vorticity that is induced by the shear. The resulting roll deformation will in turn enhance the mean-flow effects. At the same time it will be opposed by shearing planes that tend to rigidify the rolls. It is thus expected that SDC competes with ISR under shear. In fact we present simulations which show that, under the influence of shear flow, RB convection spontaneously forms a banded structure characterizing the coexistence of SDC and ISR.

Our paper is constructed as follows. In the next section we introduce model equations for RB convection under applied shear flow. These are suitably generalized Swift-Hohenberg (SH) equations [9] including the mean flow and shear flow. We solve numerically a cell-dynamical-system [10] model (motivated by the SH-model description) that is expected to be appropriate for our problem. In Sec. III we show the results of the simulation. Section IV contains a general discussion of our results.

II. MODEL EQUATIONS

A. The generalized Swift-Hohenberg model under shear flow

A simplified model of the transition to roll patterns was introduced by Swift and Hohenberg [9]. It is a two-dimensional theory involving a real order parameter $\psi(x,y,t)$, which describes the slow (spatial and temporal) variation of the vertical component of the velocity and the temperature. To study the effects of shear on the horizontal structure, we extend the SH equation by including a horizontal velocity driven by distortions of the patterns as follows:

$$\partial_t \psi = \epsilon\psi - (\nabla^2 + k_m^2)^2\psi - \tilde{g}\psi^3 - \boldsymbol{v}\cdot\boldsymbol{\nabla}\psi, \tag{1}$$

where ϵ is the reduced control parameter with the transition to rolls occurring for $\epsilon > 0$. The divergence-free horizontal velocity $\boldsymbol{v}$ is completely defined by the vertical vorticity $\boldsymbol{\Omega} = \boldsymbol{\nabla}\times\boldsymbol{v}$. We assume the general form of vorticity driving given by Manneville [11]:

$$(\tau\partial_t - \eta\nabla^2)\boldsymbol{\Omega} = g_m \boldsymbol{\nabla}\psi\times\boldsymbol{\nabla}(\nabla^2\psi). \tag{2}$$

*Electronic address: shiway@hiei.kit.ac.jp

The coefficient g_m represents the strength of the hydrodynamic coupling between $\boldsymbol{v}$ and the field ψ. This coupling is crucial for persistent SDC [12]. The first term on the left-hand side represents the inertial effects of the fluid, while the second term comes from the viscous dissipation due to horizontal gradients of the flow. For a slowly varying $\boldsymbol{\Omega}$ we may take $\tau=0$ for simplicity (the so-called passive vorticity case [13]).

In the present paper we consider the case of a steady shear flow where the average flow $\boldsymbol{u}\equiv\langle\boldsymbol{v}\rangle$ is given by

$$\boldsymbol{u}=sy\boldsymbol{e}_x, \tag{3}$$

with s being the shear rate and $\boldsymbol{e}_x$ the unit vector along the x axis. Writing $\boldsymbol{v}=\boldsymbol{u}+\boldsymbol{v}'$, we introduce the ''intrinsic'' vorticity $\boldsymbol{\Omega}'$, defined by $\boldsymbol{\Omega}'=\boldsymbol{\nabla}\times\boldsymbol{v}'$. Then $\boldsymbol{v}'$ is driven through the equation

$$\nabla^2\boldsymbol{\Omega}'=g\boldsymbol{\nabla}(\nabla^2\psi)\times\boldsymbol{\nabla}\psi, \tag{4}$$

where $g\equiv g_m/\eta$.

Finally, to account for the damping of the horizontal flow by the viscous coupling to the top and bottom plates, we follow Refs. [2,11] to modify Eq. (4) phenomenologically as

$$(\nabla^2-c^2)\boldsymbol{\Omega}'=g\boldsymbol{\nabla}(\nabla^2\psi)\times\boldsymbol{\nabla}\psi, \tag{5}$$

with c^2 an $O(1)$ constant serving as a measure for the damping effect.

Let us introduce the vertical vorticity potential ζ, defined by $\boldsymbol{e}_z\cdot\boldsymbol{\Omega}'=-\nabla^2\zeta$, $\boldsymbol{e}_z$ being the unit vector in the z direction, so that $\boldsymbol{v}'=(\partial_y\zeta,-\partial_x\zeta)$. It then yields

$$\partial_t\psi=\epsilon\psi-(\nabla^2+k_m^2)^2\psi-\tilde{g}\psi^3-sy\partial_x\psi-\boldsymbol{\nabla}\zeta\wedge\nabla\psi, \tag{6}$$

$$(c^2-\nabla^2)\nabla^2\zeta=g\boldsymbol{\nabla}\nabla^2\psi\wedge\nabla\psi, \tag{7}$$

where $\boldsymbol{\nabla}f\wedge\boldsymbol{\nabla}h\equiv\partial f/\partial x\ \partial h/\partial y-\partial f/\partial y\ \partial h/\partial x$. The model that will be studied in what follows is defined by Eqs. (6) and (7). Note that the term ∇^2 in $c^2-\nabla^2$ serves to reduce the importance of higher-wave-number modes in the vorticity field [14].

B. Method of simulations

Instead of using the conventional discretization algorithm for the partial differential equations (PDEs) (6) and (7), we employ the cell-dynamical-system (CDS) method on a square lattice [10]. The CDS method is to construct *ab initio* the corresponding space-time discrete model at the mesoscopic level. Hence the discretizaton mesh sizes are too coarse to give a numerical solution that accurately shadows the solution of the original PDEs. However, it is now amply supported that CDS modeling is a computationally efficient method to attain the late stage dynamics of the systems under study. The CDS model corresponding to Eq. (6) in the absence of hydrodynamic coupling (i.e., for $g=0$) is

$$\psi(\boldsymbol{n},t+1)=\mathcal{J}(\boldsymbol{n},t)-sn_y[\partial_x]_d\psi(\boldsymbol{n},t). \tag{8}$$

Here $\psi(\boldsymbol{n},t)$ is the order parameter at time t in the cell at the lattice point $\boldsymbol{n}=(n_x,n_y)$, where n_x and n_y are integers with $1\leqslant n_x\leqslant L_x, 1\leqslant n_y\leqslant L_y$, and

$$\mathcal{J}\equiv A\tanh\psi-L[[\psi]_\kappa]_\kappa \tag{9}$$

is the effective chemical potential corresponding to the first three terms on the right-hand side of Eq. (6). The parameters A, L, and κ set the units used in the CDS dynamics, and

$$[X]_\kappa=\langle\langle X\rangle\rangle-\kappa X, \tag{10}$$

where the double angular brackets denote the isotropized average of a neighborhood of cells:

$$\langle\langle X\rangle\rangle=\frac{1}{6}\sum X(\text{nearest}-\text{neighbor cells})+\frac{1}{12}\sum X(\text{next}-\text{nearest}-\text{neighbor cells}). \tag{11}$$

In Eq. (8), $[\mathcal{O}]_d$ denotes the discrete version of the enclosed operator $\mathcal{O}$, and the discrete gradient is center-difference evaluated.

We apply a predictor-corrector algorithm to Eqs. (6) and (7) to upgrade the order-parameter field; namely, we first predict the order-parameter field based on Eq. (8), and then it is corrected using the predicted value of ψ to evaluate ζ on the right-hand side of Eq. (6):

$$\psi^*(\boldsymbol{n})\equiv\mathcal{J}(\boldsymbol{n},t)-sn_y[\partial_x]_d\psi(\boldsymbol{n},t), \tag{12}$$

$$(c^2-[\nabla^2]_d)[\nabla^2]_d\zeta(\boldsymbol{n},t)=g[\boldsymbol{\nabla}]_d[\nabla^2]_d\psi^*(\boldsymbol{n})\wedge[\boldsymbol{\nabla}]_d\psi^*(\boldsymbol{n}), \tag{13}$$

$$\psi(\boldsymbol{n},t+1)=\psi^*(\boldsymbol{n})-[\boldsymbol{\nabla}]_d\zeta(\boldsymbol{n},t)\wedge[\boldsymbol{\nabla}]_d\psi^*(\boldsymbol{n}). \tag{14}$$

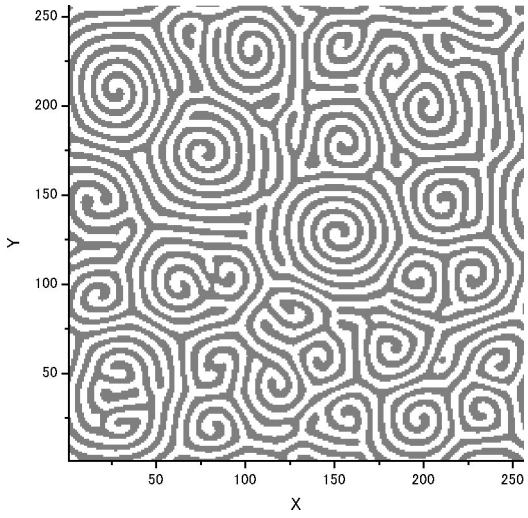

FIG. 1. Snapshot of the SDC state at $t=30\,000$ in numerical simulations of Eqs. (12)–(14). The white regions denote positive values of the order parameter ψ and the gray ones negative ψ.

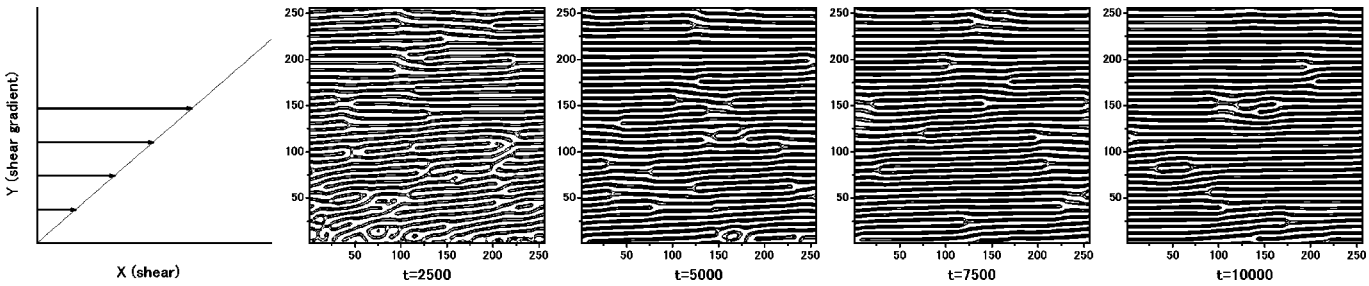

FIG. 2. Domain growth under shear flow with shear rate $s=0.002$ in response to random initial conditions. The shear direction and the shear gradient direction are shown relative to the assigned coordinate system. At the bottom of each panel the time step is shown.

In order to solve the implicit equation (13) for ζ, we use the pseudospectral technique with a fast Fourier transform method, and for the Laplacian we use the identification [15] $[\nabla^2]_d X = 3(\langle\langle X\rangle\rangle - X)$.

It should be remarked here that caution is required in the computation of Fourier transforms (see, e.g., [16]) because the boundary condition in the presence of the shear flow given by Eq. (3) becomes [17]

$$\psi(n_x, n_y, t) = \psi(n_x + N_x L_x + \gamma(t) N_y L_y, n_y + N_y L_y, t) \tag{15}$$

with arbitrary integers N_x and N_y, and $\gamma(t) \equiv st$ being the shear strain.

III. RESULTS

We have studied the domain growth of convection patterns by computer simulations of Eqs. (12)–(14) with fixed parameters $c^2=2$, $L=0.8$, $\kappa=0.7$, and $g=20$. We have explored the shear effects for several values of A and s. Unless otherwise specified, the initial conditions are a random uniform distribution of the ψ's in the range $[-0.1,0.1]$. We have studied several systems with $L_x \times L_y = 256\times 256$, 512×512, and 512×1024 to investigate the finite-size effect. (According to the linear analysis of Eq. (9), the diameter of a roll (d) is estimated to be $d=\pi/k_m$ with $k_m = \arccos[(3\kappa-1)/2]$. Hence the aspect ratio (Γ) of the systems studied is $(\Gamma_x, \Gamma_y) \equiv (L_x/2d, L_y/2d) = (40,40), (81,81), (81,161)$, respectively.) We observed that all runs were consistent with the qualitative behavior reported below.

A. Shear deformation and alignment

In the absence of shear flow but with hydrodynamic couplings ($g=20$), we observed that the SDC state grew for $A \gtrsim 1.03$ from random initial conditions. Figure 1 shows an example of the SDC pattern for $A=1.05$. When shear is imposed and when the shear rate is substantially small, the domains growing exponentially in the initial regime are essentially unaffected by the shear, and the subsequent coarsening leads to a pattern similar to the no-shear case.

With large shear rates, however, deformation of domains dominates long before the corresponding spirals have formed. Figure 2 illustrates such a case with $s=0.002$. In order to see how the SDC pattern deforms under strong shear, we also performed simulations with the same shear rate but by imposing initially a well-developed SDC pattern. The time evolution of the pattern is shown in Fig. 3. In the initial stage the spirals are simply elongated along the bisec-

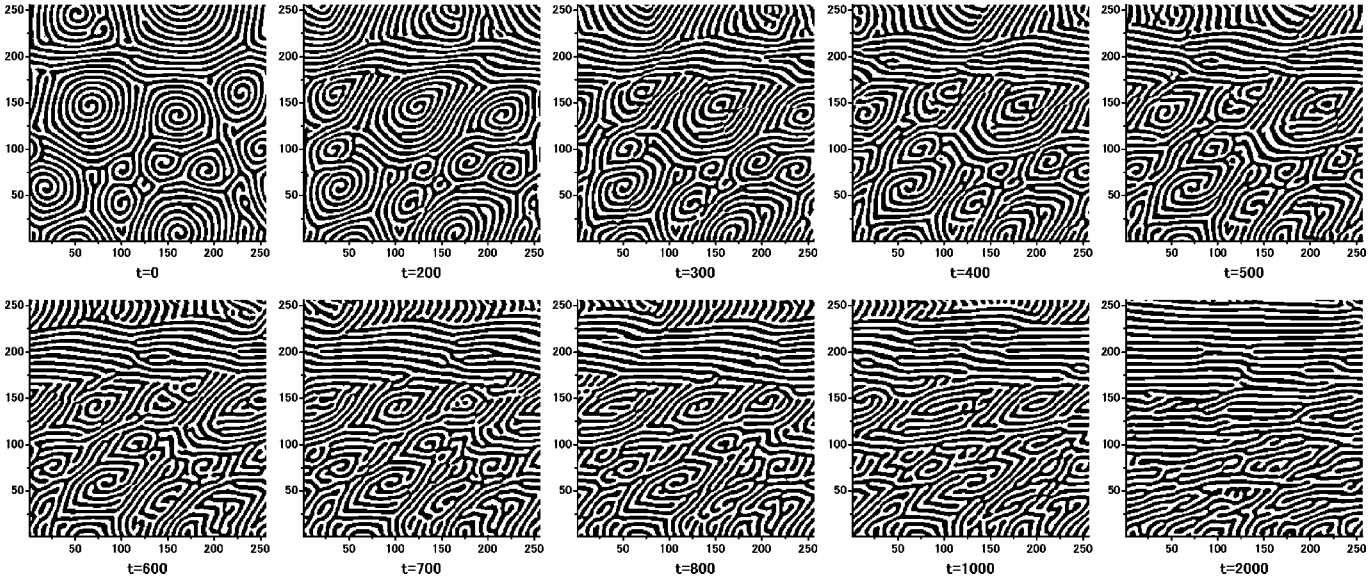

FIG. 3. Time evolution of the initially imposed SDC pattern in the presence of shear with $s=0.002$.

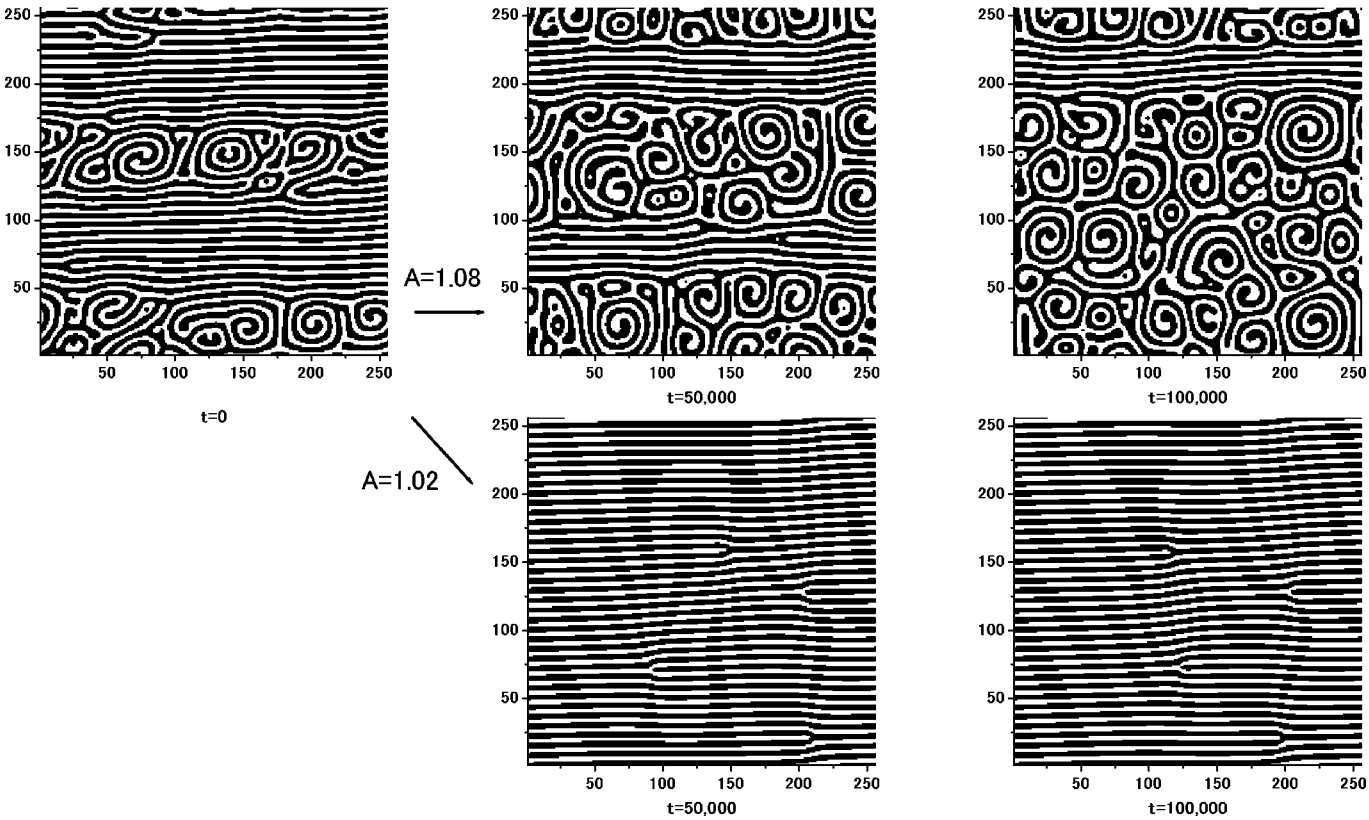

FIG. 4. Shear banding observed at $t=10^5$ for $A=1.05$ under shear of $s=5\times10^{-4}$ (the upper left panel). Shown on the right is the time evolution of the shear band after a temperature jump to $A=1.08$ or temperature quench to $A=1.02$ is imposed. The elapsed time step after the temperature change is shown at the bottom.

tor of the x and y axes by the deformation component of the shear flow. At intermediate times the average direction of the patterns rotates and becomes more aligned with the flow. In the meanwhile the stretched spiral domains rupture to form stripes. At large times, regions with stripes aligned with the flow fill the whole space.

B. Shear banding

For intermediate strengths of shear, we find that a banded structure is spontaneously formed, exhibiting the coexistence of rolls and spirals. It is shown in Fig. 4. The nonequilibrium coexistence between phases of different symmetry is commonly referred to as shear banding, and has been reported frequently (albeit little is known about the underlying mechanism determining this coexistence) in a variety of soft matter such as colloid crystals and wormlike micelles under shear (see Ref. [18] for a recent review). As will be shown in the next subsection, this banded structure is quite long lived, indicating a metastable state.

Use of the shear band structure can give additional confirmation of the before-mentioned statement concerning which of SDC and ISR is the generic attractor starting from random initial conditions; namely, we used this morphology as an initial condition for a simulation and abruptly changed the value of A (corresponding to a ''temperature'' jump). We observed that, depending on which basin of attractor the temperature jump is made into, either SDC or ISR first appear at the SDC-ISR interface and gradually cover the whole space. As illustrated in Fig. 4, SDC is an intrinsic state of convection for $A\gtrsim1.03$.

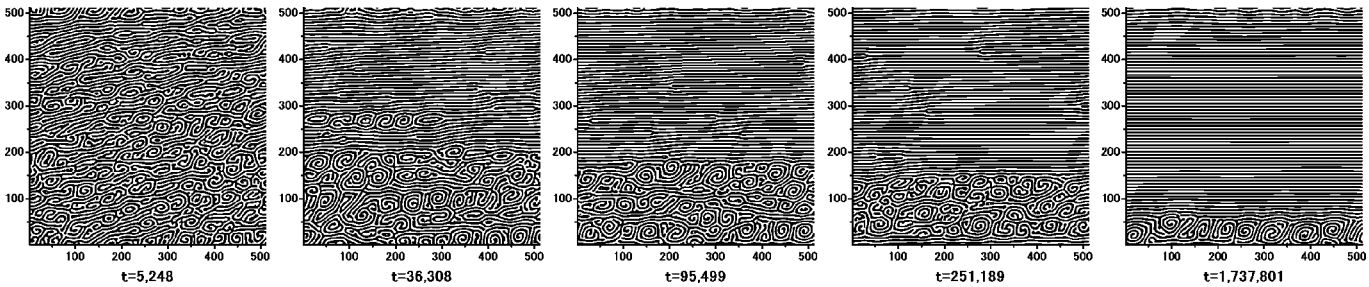

FIG. 5. Snapshots of the ψ field at various times from random initial conditions with $A=1.05$ and $g=20$ for $s=5\times10^{-4}$.

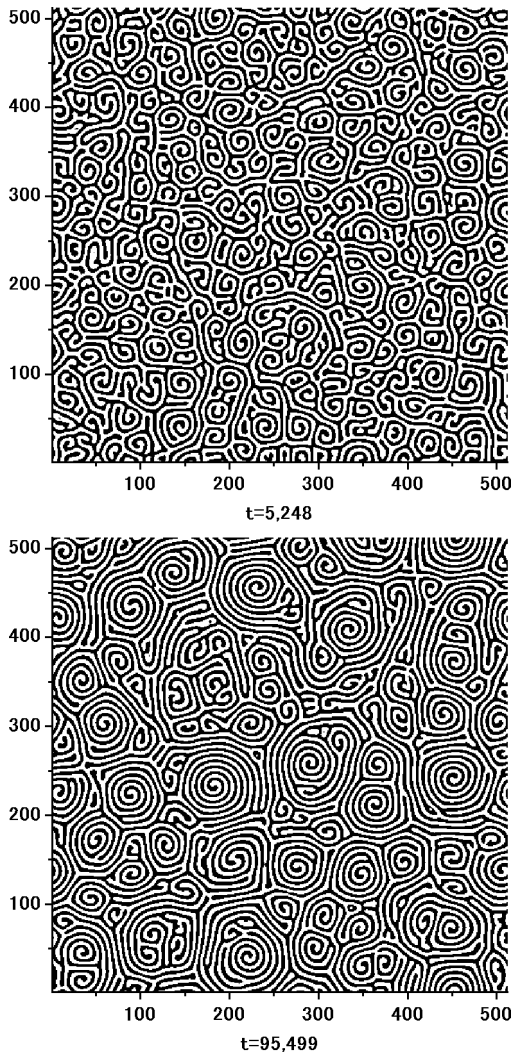

FIG. 6. Evolution of SDC without shear. The other conditions are the same as for Fig. 5.

C. Metastability

Simulations showed that the shear banding existed for a very long time. This is illustrated in Fig. 5, where a square cell of $\Gamma=81$ is used with $s=5\times10^{-4}$. Even at 1.7×10^{6} time steps after shearing had started, the coexistence remained. (Note that the horizontal diffusion time scale is given by $4\Gamma^2\approx26\,000$ in units of the vertical viscous time scale.) For comparison, evolution of SDC in the absence of the shear flow but with the other parameters being the same is shown in Fig. 6. Clearly the asymptotic state without shear in this case is SDC. These results suggest metastability of the banded structure.

The metastability of the coexistence of SDC and ISR was verified by a shear cessation experiment (numerical) as follows. After establishing well-defined bands under shear flow, we turned off the shear and saw how the system chose between SDC and ISR. The observed evolution of SDC invading the ISR region is shown in Fig. 7. The SDC state grew at the SDC/ISR interfaces, gradually drifting toward the ISR region. This process continued until the SDC filled the entire plane. The invasion into ISR regions through the propagation of almost flat fronts in our simulation compares remarkably well with the experimental observations [5,6]. We remark, however, that in those experiments the SDC/ISR boundary was triggered by a slight inhomogeneity on the sidewall of the convection cell.

We quantify the competition between the two states by monitoring the spatial average of the intrinsic vertical vorticity $\Omega_z'\equiv S^{-1}\int d\mathbf{r}\boldsymbol{e}_z\cdot\boldsymbol{\Omega}'$, where S is the area of the system. We associate the growth in $|\Omega_z'|$ with the formation of spiral morphology. Figure 8 shows the time dependence of the absolute value of Ω_z' that we obtained from the shear cessation simulation of Fig. 7. After cessation $|\Omega_z'|$ rapidly decreased from the initial value (given by the horizontal dashed line) to the value $\Omega_i\approx0.003\,94$. The value of $|\Omega_z'|$ remained unchanged over very long times, revealing the existence of an incubation period for the coarsening (of SDC) process. It then starts to increase and reaches the constant value $\Omega_f\approx0.008\,08$, indicating that the SDC fronts start to move into the ISR region and the system is approaching a state full of SDC. The same stationary limit Ω_f is obtained for SDC formation from random initial conditions (open circles in Fig. 8). These features, together with the coexistence of two different phases, suggest that the domain coarsening in this case is the nucleation and growth process. In fact, as plotted by the solid curve in Fig. 8, the sigmoidal shape of the $|\Omega_z'|$ curve is well represented by the Avrami form [19]

$$|\Omega_z'(t)|=[1-X(t)]\Omega_i+X(t)\Omega_f, \tag{16}$$

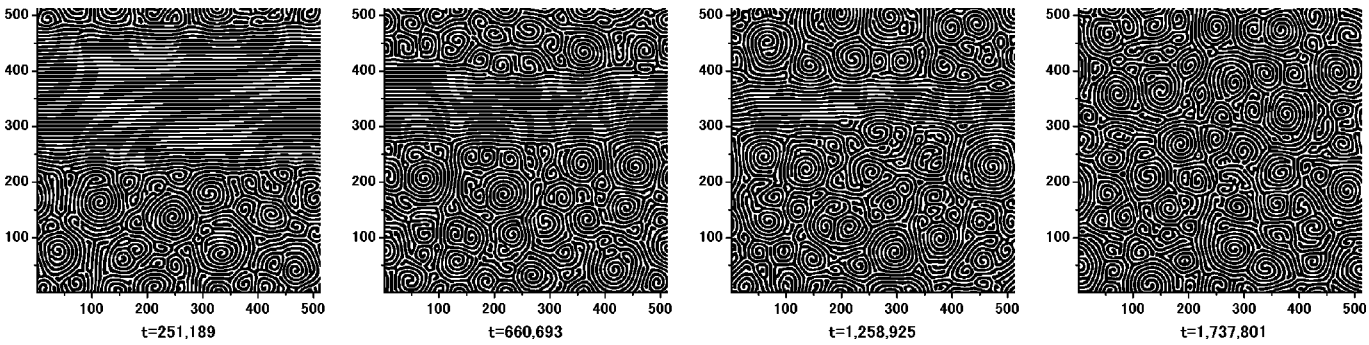

FIG. 7. Time evolution of the shear band after cessation of shearing. The initial pattern at $t=0$ is the pattern attained after $t=95\,499$ time steps under shear of $s=5\times10^{-4}$ as given in Fig. 5. The elapsed time after the cessation is given at the bottom of each panel.

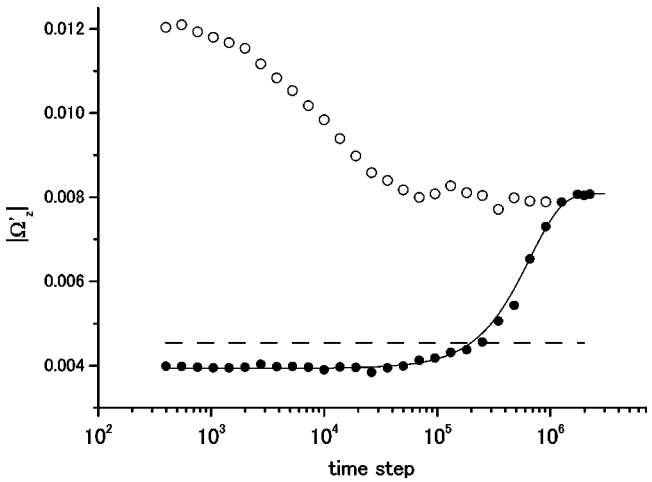

FIG. 8. Time dependence of the strength of the intrinsic vertical vorticity Ω'_z in response to the shear cessation (filled circles) as described in Fig. 7. The horizontal dashed line denotes the value of $|\Omega'_z|$ just after the cessation. The solid curve is the best fit to the data using the Avrami form [see Eqs. (16) and (17)]. Also shown by open circles is the time evolution of $|\Omega'_z|$ in the absence of shear after starting with random initial conditions.

with

$$X(t)=1-\exp[-(t/\tau)^n]. \tag{17}$$

The quantity $X(t)$ represents the volume fraction of SDC at t, where τ and n are constants. The so-called Avrami exponent n is determined in our case to be $n\approx 1.5$. Considering the limited accuracy of our data, this value is not inconsistent with the results that the front propagation is local to the neighborhood of the flat interface and the front velocity is approximately independent of time [6]. However, it should be remarked that the classification of the nucleation kinetics with the Avrami exponents may be misleading due to many specific assumptions that the Avrami theory is based on (see, e.g., Ref. [20]). Hence we here only take the viewpoint that growth characterized by Avrami-like kinetics (16) is consistent with nucleation and growth. Interpretation in terms of this nucleation and growth dynamics is a strong indication of the metastability of the shear band structure.

IV. DISCUSSION

We have studied the model equations that govern the formation of SDC and ISR under a steady shear. We found a shear banding where both SDC and ISR states coexist. The existence of a prolonged transient behavior of the vertical vorticity could be interpreted as an indication of metastability of this shear-induced structure.

In the present paper, we considered the dynamic response of the spiral patterns to shear deformation. It would be interesting to examine how such deformation is reflected in rheological properties, because it is well known that the rheological properties are very sensitive to the appearance and disappearance of spatial orders. We anticipate that a variety of anomalous dynamic properties will be observed. For instance, one might ask how distortions of spiral geometries affect the stress-strain relation of these structures. Here we merely write down the expression of the stress tensor $\sigma_{\alpha\beta}$ for the system described by Eq. (1). It may be derived by using the method described in Ref. [21] and is given by

$$\sigma_{\alpha\beta}(t)=-\frac{2}{V}\sum_{\boldsymbol{k}}\frac{k_\alpha k_\beta}{k_m^2}(k^2-k_m^2)S(\boldsymbol{k},t), \tag{18}$$

with the isotropic contributions being dropped out. Here $S(\boldsymbol{k},t)\equiv\langle|\psi(\boldsymbol{k},t)|^2\rangle$ is the structure factor calculated from the Fourier component $\psi(\boldsymbol{k},t)$ of the order parameter, and V is the system volume. The expression (18) should be useful in elucidating the nature of SDC, and we hope to be able to report on this development in the future.

The ordering kinetics of spiral pattern formation in the absence of shear flow is of great interest in its own right and deserves further study. As in roll formation, coarsening toward the SDC state following a rapid ''quench'' in temperature exhibits a long-time dynamics. This may be inferred from Fig. 8 (open circles). (From Fig. 8 we find that $|\Omega'_z|$ relaxes to the plateau value in proportion to $t^{-\beta}$ with $\beta\approx 0.3$. We note, however, that this value of the exponent should not be taken too seriously because our present numerical data are of limited accuracy.) In view of the fact that no successful theoretical understanding is yet available for the ordering dynamics of roll patterns [22], it is certainly important to broaden the question to systems in which the spatially periodic state is different from but nonetheless closely related to roll patterns. For example, one may ask whether there is any length scale characterizing the growth of the SDC regions, and if it should exist the question of how the length scale grows with time becomes relevant.

ACKNOWLEDGMENT

The author is grateful to Shin Sakurai for conveying to him the experimentalist view of the Avrami theory.

[1] For a review, see M. C. Cross and P. C. Hohenberg, Rev. Mod. Phys. **65**, 851 (1993).
[2] E. D. Siggia and A. Zippelius, Phys. Rev. Lett. **47**, 835 (1981); A. Zippelius and E. D. Siggia, Phys. Fluids **26**, 2905 (1983).
[3] S. W. Morris, E. Bodenschatz, D. S. Cannell, and G. Ahlers, Phys. Rev. Lett. **71**, 2026 (1993); for subsequent developments, see E. Bodenschatz, W. Pesch, and G. Ahlers, Annu. Rev. Fluid Mech. **32**, 709 (2000).
[4] R. M. Clever and F. H. Busse, J. Fluid Mech. **65**, 625 (1974).
[5] R. V. Cakmur, D. A. Egolf, B. B. Plapp, and E. Bodenschatz, Phys. Rev. Lett. **79**, 1853 (1997).
[6] I. V. Melnikov, D. A. Egolf, S. Jeanjean, B. B. Plapp, and E. Bodenschatz, in *Stochastic Dynamics and Pattern Formation in Biological and Complex Systems*, edited by S. Kim, K. J.

Lee, and W. Sung, AIP Conf. Proc. No. 501, AIP, Melville, NY, 2000, p. 36.
[7] A. Onuki, J. Phys.: Condens. Matter **9**, 6119 (1997), and references cited therein.
[8] R. E. Kelly, Adv. Appl. Mech. **31**, 35 (1994).
[9] J. Swift and P. C. Hohenberg, Phys. Rev. A **15**, 319 (1977); P. C. Hohenberg and J. B. Swift, *ibid.* **46**, 4773 (1992).
[10] Y. Oono and S. Puri, Phys. Rev. Lett. **58**, 836 (1987); Y. Oono and Y. Shiwa, Mod. Phys. Lett. B **1**, 49 (1987); for more recent references, see A. Shinozaki and Y. Oono, Phys. Rev. E **48**, 2622 (1993).
[11] P. Manneville, J. Phys. (Paris) **44**, 759 (1983).
[12] M. Bestehorn, M. Neufeld, R. Friedrich, and H. Haken, Phys. Rev. E **50**, 625 (1994).
[13] M. C. Cross and Y. Tu, Phys. Rev. Lett. **75**, 834 (1995).
[14] M. C. Cross, Physica D **97**, 65 (1996).
[15] P. I. C. Teixeira and B. M. Mulder, Phys. Rev. E **55**, 3789 (1997); Y. Oono, *ibid.* **55**, 3792 (1997).
[16] T. Ohta, Y. Enomoto, J. L. Harden, and M. Doi, Macromolecules **26**, 4928 (1993).
[17] A. W. Lees and S. F. Edwards, J. Phys. C **5**, 1921 (1972).
[18] S. Butler and P. Harrowell, Nature (London) **415**, 1008 (2002).
[19] M. Avrami, J. Chem. Phys. **7**, 1103 (1939).
[20] P. Uebele and H. Hermann, Modell. Simul. Mater. Sci. Eng. **4**, 203 (1996).
[21] K. Kawasaki and T. Ohta, Physica A **139**, 223 (1986).
[22] For the current status of this research, see, e.g., D. Boyer and J. Viñals, Phys. Rev. E **64**, 050101(R) (2001).